The Meteoritical Society

Meteoritics & Planetary Science 42, Nr 4/5, 769–778 (2007)
Abstract available online at http://meteoritics.org

Clast fabric examination of impact-generated breccias, borehole LB-07A, Bosumtwi, Ghana

William A. MORRIS*, Hernan UGALDE, Christina CLARK, and Brett MILES

McMaster Applied Geophysics and Geological Imaging Consortium, School of Geography and Earth Sciences, McMaster University, 1280 Main Street West, Hamilton, Ontario, L8S 4K1, Canada
*Corresponding author. E-mail: morriswa@mcmaster.ca

(Received 25 July 2006; revision accepted 23 December 2006)

Abstract–An impact event always creates a cloud of ejecta generated through excavation of the target. Subsequent in-filling of the void by crater-fill deposits provides a record of post-impact processes. Full-core digital photographic scans of core segments from borehole LB-07 in the Bosumtwi impact crater provide a complete record of the in-fill process. The shape, orientation, and size of clasts within the impact breccia were measured using a best-fit ellipsoid approach. Clast size and variance, together with clast orientation data, suggest the impact breccias at Bosumtwi can be divided into a simple two-fold subdivision that loosely agrees with the lithological zonation of a lower monomict breccia overlain by a polymict breccia. The lower unit is characterized by a uniform and finer-grained clast size together with a uniform flat-lying clast orientation. The boundary between the two zones is defined by a sharp increase in clast size. The upper zone shows an average increase in clast size with decreasing depth, but full grain size spectrum together with increased grain size deviation suggest that this is a result of mixing between two populations with different grain size distribution. The main population of clasts shows an incremental decrease of clast size with decreasing depth. The upper zone also contains weakly defined shallowly dipping clast fabrics, which may be suggestive of horizontal transport or deposition onto an inclined surface.

INTRODUCTION

Ejecta material, which accumulates as crater fills, often displays a crude stratification that is produced by the interlayering of distinct lithological phases (Masaitis 2005). The preserved sequence of crater-fill lithologies provides a record of spatially varying transportation and accumulation processes in the ejecta cloud. Subsequent localized variations in post-depositional cooling and crystallization processes can modify any primary depositional fabrics (Knauth et al. 2005; Bringmeier 1994). Masaitis (2005) suggests that most crater-fill deposits conform to a simple three-layer sequence. From bottom to top the three layers comprise a basal layer of "coarse lithic breccias," an intermediate layer of "suevite and tagamite," and an upper layer of "fine grained lithic breccia." Bringmeier (1994) suggests that while transport mechanisms associated with emplacement of the lithic breccias are well understood, transport models to explain emplacement of suevite are "more diverse." At issue is the degree of horizontal versus vertical transport. Reporting results from a study of the suevite at the Ries impact crater, Bringmeier (1994) states "movement of the suevite of Otting must at least be horizontal, perhaps in the form of a suevitic flow." In the present study of clast fabric in impactites from the Bosumtwi crater we determine if this explanation is generally applicable, or the interpretation presented by Bringmeier (1994) will have to be re-examined.

The morphology of the clasts generated by a meteorite impact event is at least partially controlled by the lithology of the target. Should the impact produce an oblate or prolate clast morphology, then upon accumulation, the clasts will almost certainly acquire a fabric that is a consequence of the mode of transport. Lithologic logging of core from Lake Bosumtwi borehole LB-07A records a sequence of monomict, polymict breccias interbedded with layers of suevite (Coney et al. 2007; Koeberl et al. 2007). If these lithologies are the result of different transport mechanisms they should have different fabrics. To investigate the presence of any systematic changes in clast fabric with depth we have examined the scanned photographic records of all core fragments from borehole LB-07A. Borehole LB-08A had insufficient length of crater-fill material to warrant study (Koeberl et al. 2007). Two aspects of the clast fabric (grain size and clast orientation) were measured on each core

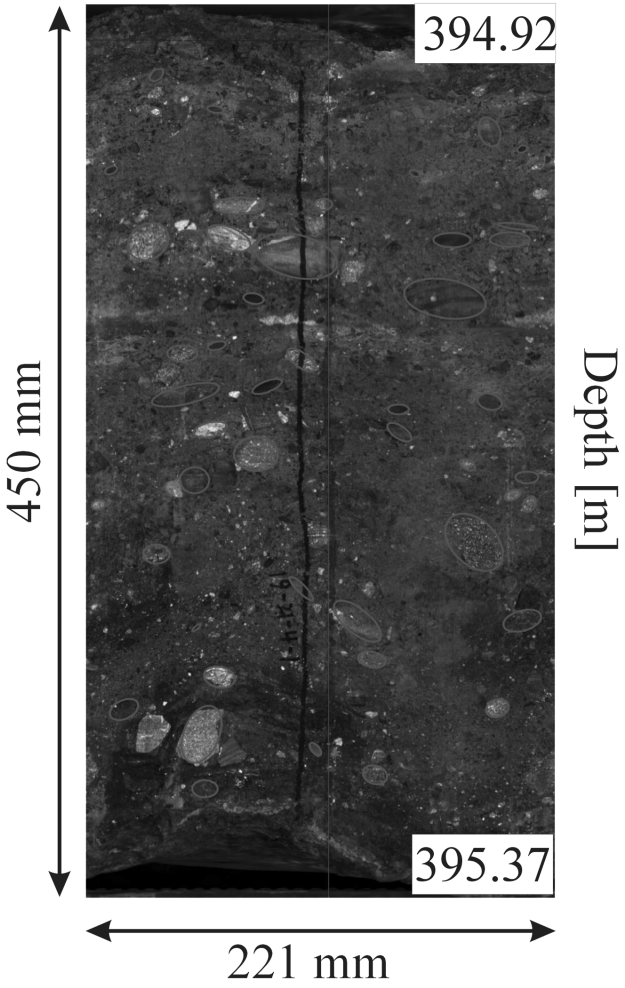

Fig. 1. A complete core scan of core segment B019R021.BCDP-7A.4.1 (GFZ nomenclature: Hole LB-07A, box 19, row 21, segment 4.1), located at a depth interval of 394.92–395.37 m. Clast outlines defined by best-fit ellipse are defined by white ellipses. Reference line on core (irregular dark line) provides absolute reference point. Up direction of core is upward in the figure.

segment from the photographic record of LB-07A. Since the measurements were performed in advance of receiving the lithologic log for LB-07A, no attempt was made to subdivide the results in terms of the proposed lithologic boundaries. Rather, the results are presented in terms of mean fabric parameters for each core segment irrespective of lithology. It is quite possible that an individual core segment could include more than one lithologic unit. Detailed geological logs as used in this presentation are based on work of Coney et al. (2007) and Deutsch et al. (2007). A previous study of the clast fabric present in a piece of the Bosumtwi impactite has been reported by Koeberl et al. (2002). Using high-resolution X-ray computed tomography (HRXCT), Koeberl et al. (2002) were able to discriminate individual clast lithologies with a minimum discernible clast size of 0.5 mm. Comparing the HRXCT data with macroscopic and microscopic petrography, Koeberl et al. (2002) show that it is possible to discriminate granite, schist, and aplite fragments. Interspersed with these rock fragments are impact melt and glass fragments. Figure 6 of Koeberl et al. (2002) suggests that many of the granite and schist clast fragments have a preferred oblate form. Justifiably no attempt was made to determine if these clasts had any preferred orientation. Since the orientation of the original sample was unknown, even if a fabric were calculated from the HRXCT observations it would not be possible to establish the trajectory of the fabric in an absolute reference frame. In this study, we report results based on a study of core sections obtained from LB-07A. The inclination of each segment of core, which can be easily derived from the borehole deviation survey (Morris et al. 2007), is within 10° of vertical. No correction for hole inclination was needed. Each core segment was marked with a red reference line (Fig. 1). Within each core segment the position of each clast was established with respect to this local reference line. However, the reference line does not appear at the same point on every image; therefore, to bring all the core segments into a common absolute reference frame requires additional information. Since the borehole televiewer imagery is referenced to geomagnetic north it is possible to bring the optical photographic images into an absolute reference frame by comparing the images (Hunze and Wonik 2007).

Karatson et al. (2002) provide an excellent review of the application of photo-imaging to clast fabric orientation estimation. Specific problems identified by Karatson et al. (2002) include the effect of clast size, the number of clasts, and the bias introduced by view angle. Most of the imagery analyzed by Karatson et al. (2002) used one view plane ideally chosen to be the plane of maximum fabric. This is the first study to present a detailed analysis of clast fabric as revealed by digital optical photography of oriented core samples. In this situation there is no single oriented plane. Rather, the full circumferential image contains a complete view of the fabric in the vertical plane. The objective of the present study was to determine if the different lithological units independently identified on the basis of mineralogical variations are associated with changes in clast orientation and clast size.

CLAST FABRICS

The clast fabric descriptors in this study were derived from the digital photographic scans of all coherent core segments from the impactite units sampled in borehole LB-07A. The photographic scans were all performed at the International Continental Scientific Drilling Program (ICDP) research facility at the GeoForschungsZentrum (GFZ) in Potsdam, Germany, in December 2004. Each scan was performed using a collimated viewer attached to a digital camera. The core was mechanically rotated under computer control to produce a complete circumferential scan. It is

assumed that the long axis of each core segment is essentially subparallel to the locally observed trajectory of the borehole at the point of sampling. All the core segments are truly cylindrical. All images were acquired using the same camera settings and same distance between the sample and the image plane. All of the images therefore should have approximately the same scale. Minor fluctuations in core diameter (nominally 70 mm) would not have any significant impact on the resulting image.

Following the nomenclature used by Sahagian and Proussevitch (1998), impactites would represent a mixture between a polydispersal (clasts have same shape but different size) and a multidispersal system (clasts have different shape and size). It is reasonable to assume that clasts derived from the same lithology will have the same general morphology. The size of the clasts might vary, but given uniform sedimentation processes one might also expect a uniformity of clast size. The complete circumferential scan is equivalent to having a number of 2-D plane images around the morphology of a 3-D entity (the core segment), where all the 2-D planes are vertical and parallel to the long axis of the core. From this configuration it is possible to determine if there is any strongly preferred alignment of fabric clasts. Consider the simple geometrical models displayed in Fig. 2. Clast morphology can vary between a limited number of extreme endmembers:

a. Square: cube or sphere. Each orthogonal axis of the clast is of equal length.
b. Prolate: elongate ellipsoid or rod. Long axis of the object is much greater than the two other axes.
c. Oblate: flattened ellipsoid or slab. Axes in horizontal plane are of near equal length, while vertical axis is much less.

Differences between ellipsoids and rectangular bodies would arise depending on initial fracturing and subsequent abrasion. The observed size of a spherical or ellipsoidal clast will vary depending on the position of the intersection plane (core surface) relative to the center of the spherical clast (Figs. 2a and 2b); whereas for the sphere and the cube the observed clast shape is totally independent of view direction (Figs. 2c and 2d). As noted by Sahagian and Proussevitch (1998), the probability of cutting a sphere through its largest diameter is 61%, irrespective of the sphere diameter. All other intersections of the sphere (and ellipsoid) will have smaller diameter. This would be reflected in grain-size distribution plots by a normal distribution that is skewed towards finer grain sizes. A clast having more rectilinear boundaries will not show the same distribution of grain-size variation with view direction (Fig. 2).

In geological terms, a series of collinear prolate objects corresponds to a lineation. From the perspective of a core segment this fabric would result in one view, parallel to the lineation, that will show little or no preferred grain orientation to the orthogonal view, and which would maximize the observed lineation. On the other hand, a series of co-planar oblate objects in geological terms corresponds to a foliation. All views of this type of fabric must exhibit some preferred clast alignment. It has been common geological practice to measure the direction of clast elongation on a number of variable dipping bedrock surfaces to determine the absolute orientation of the clast fabric (McDonald and Palmer 1990; Ort et al. 1999).

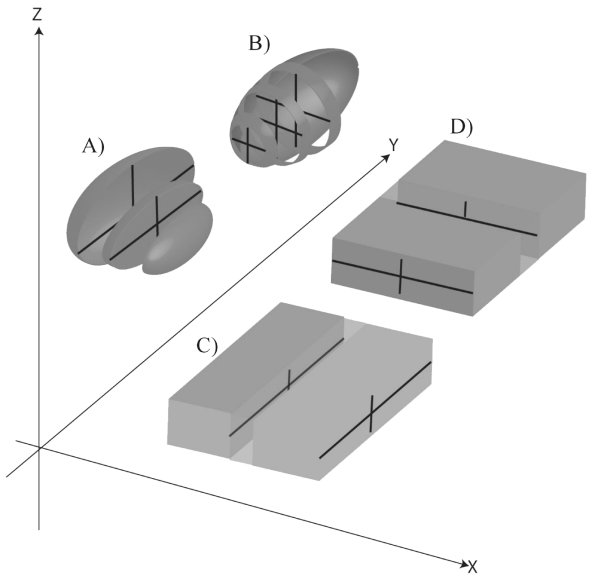

Fig. 2. A clast morphology diagram that demonstrates how observed clast shape is controlled by location of intersection plane and primary clast shape, and how apparent clast size can be impacted by position of intersection plane relative to clast centroid. Clast distribution pattern is affected by primary shape of clast and by distribution of clasts. A fabric can be produced by a series of elongate clasts, or a preferred alignment of a number of equant clasts. a) Ellipsoidal clast with intersection planes parallel to YZ. b) Ellipsoidal clast with intersection planes parallel to XZ. Both (a) and (b) show how the observed size of a spherical or ellipsoidal clast will vary depending on the position of the intersection plane relative to the centre of the spherical clast. c) Cubic clast with intersection planes parallel to YZ. d) Cubic clast with intersection planes parallel to XZ. Both (c) and (d) show how for the sphere and the cube the observed clast shape is totally independent of view direction.

Simple geometrical considerations require that for a foliation the orientation of the clast alignment must also exhibit a symmetrical sinusoidal variation in trend, relative to position around the circumference of the core segment (Krumbein 1939). This constraint provides some simple tests. First, if a single preferred clast orientation is present in a core segment, then knowing the relative position of each observation point the fabric inclination must exhibit a single sinusoidal distribution. Second, if there are significant differences in the magnitude of the orthogonal axes of the clasts then the axial ratio should also exhibit a sinusoidal variation. Third, the sinsusoidal variations associated with axial ratio must have the same phase as the sinusoidal

variations associated with clast inclination. When clast inclination is near vertical or near horizontal, it becomes difficult to detect axial ratio variations for respectively prolate, or oblate clasts. (The single sinusoidal distribution arises as a consequence of the convention we adopted for the orientation data).

Highly deformed rocks commonly have strongly defined mineralogical and petrological fabrics. Clast orientations in sediments never exhibit a single, unique direction, but rather tend to have a variance around a preferred orientation. All rocks may have some degree of grain alignment, or layering. A technique like anisotropic magnetic susceptibility measures the summation of the contribution of all magnetic grains in the sample under examination (Ort et al. 1999; Karatson et al. 2002). This results in a specimen mean fabric. Clasts in an impact breccia present a more complex situation. If all clasts have a similar orientation then it should be possible to measure and estimate the fabric. However, where mixed fabrics are present and not only one fabric is dominant, then the separation of individual components may become impossible.

METHODOLOGY

The fundamental basis for the clast size and clast orientation data used in this study is based on modeling individual clasts using a best-fit ellipsoid routine embedded in Adobe Photoshop (v.11). No attempt was made to identify the lithological characteristics of individual clasts. The dimensions of each ellipsoid are provided by the modeling routine. The centroid point of the ellipsoid establishes the position of the observation point relative to depth in the core segment and relative to circumferential distance around the core segment. The circumferential distance was measured relative to the red line marked on each core segment. No attempt was made to examine just how well the ellipsoid approximation actually described the geometry of the clasts. This is perceived to be more problematic for the larger clasts which have more irregular outlines. Obviously it was critical that careful attention be paid to accurately establishing the size of the image. This problem was addressed by careful referencing of each core image. Photoshop also provided the orientation, or inclination, of each ellipse relative to the long axis of each core segment. The convention used in this study is that vertically oriented clasts are given an inclination of 90°, and horizontal (flat-lying) clasts are given an inclination of 0°. We differentiated clockwise and anticlockwise inclinations from the vertical into a series of 10° classes. Subhorizontal clast orientations were treated as equal and only one class was defined for this group. To examine clast-size variations we have defined a parameter, equivalent spherical grain size, which was calculated from the vector sum of the two ellipse axes. Clast elongation is simply the ratio of the two ellipse axes.

Ellipsoidal parameters (clast inclination, grain size) were measured on a number of clasts from each core segment. Only clasts readily detectable on the photographic images are used in this study—effectively, a size cut-off of 5 mm. The number of clasts measured in each core segment ranged from a low of 10 to a high of 76. Data for each parameter is defined in terms of percentage of observations for each core segment. A total of 27 core segments from core LB-07A were examined (Table 1). Clast inclination data is presented in terms of inclination versus depth. Again assuming that there is no bias in our observational data, then a single dipping fabric should define an elongate symmetrical distribution of inclination values extending from minimum to maximum inclination. Grain-size data is presented in terms of percentage number of clasts falling into geometrically incrementing grain-size classes. Following studies on volcanogenic material we have used a series of logarithmically incrementing grain-size classes. To enhance the presence of patterns within the clast inclination and grain-size data we present the results in the form of contoured percentage plots. These images were generated using the minimum curvature gridding algorithm contained within Geosoft's Oasis Montaj (version 6.4).

Given the logic outlined above for sinusoidal variations of elliptical parameters we examined each core segment for the presence of any preferred orientation in the clast fabric. The fabric calculation involved a number of steps. Photographic images of the core are presented using a simple Cartesian (X,Y) format, where Y represents depth in each core segment, and X represents circumferential distance. In searching for a fabric we are looking for a feature that exhibits an angular relationship relative to the long axis (Y) of the core segment. Hence the first transformation involves changing X to Theta. Embedded in this transformation is an adjustment for varying core diameter. The result is that individual clasts are now defined in (Theta, Y) space. We applied two approaches to test for the proposed sinusoidal variations. Our first approach is based on the observation that a single sinusoid can be approximated by a function which includes a quadratic (x^2) term. This is directly equivalent to using a second order least squares polynomial regression. Our second approach is based on some ideas that are fundamental to Fourier spectral analysis. Essentially any sinusoidal variation can be described by three simple variables: wavelength, amplitude, and phase. For this study the wavelength is fixed. We are only looking for single fabrics. Hence, the wavelength must be equivalent to one rotation of the core. Amplitude describes the inclination of the fabric. As noted above, the maximum (true) inclination is observed twice during each rotation of the core. At all other points the observed inclination will be less. Phase prescribes the location of the two inclination maxima on the circumference of the core segment. Hence we can compute the optimized match between a calculated sinusoid and the observed data by

Table 1. Rock samples analyzed.

Box/row	Core segment	Depth start (m)	Depth end (m)	Number of clasts in segment
B001R001	BCDP-7A_1.1	333.61	333.79	12
B001R001	BCDP-7A_2.1	334.34	334.47	42
B002R002	BCDP-7A_1.1	336.80	337.02	24
B003R004	BCDP-7A_1.2	341.92	342.03	10
B003R004	BCDP-7A_2.1	342.03	342.19	24
B005R007	BCDP-7A_3.2	351.44	351.72	35
B005R007	BCDP-7A_4.1	352.00	352.40	11
B005R007	BCDP-7A_5.1	352.61	352.81	42
B006R008	BCDP-7A_3.1	354.64	354.89	33
B007R009	BCDP-7A_1.3	356.39	356.59	25
B008R010	BCDP-7A_3.1	360.35	360.54	27
B009R011	BCDP-7A_2.2	363.10	363.41	45
B010R012	BCDP-7A_1.2	365.61	365.81	28
B011R013	BCDP-7A_1.1	370.06	370.53	39
B014R016	BCDP-7A_1.1	378.30	378.55	43
B015R017	BCDP-7A_5.1	382.94	383.19	56
B016R018	BCDP-7A_5.2	385.97	386.45	40
B017R019	BCDP-7A_5.1	388.73	389.33	56
B018R020	BCDP-7A_5.1	391.36	391.92	76
B019R021	BCDP-7A_4.1	394.92	395.37	49
B020R022	BCDP-7A_2.2	396.87	397.07	24
B021R023	BCDP-7A_2.1	403.88	404.45	35

allowing two variables (phase, amplitude) to change. The Solver capability embedded in Microsoft Excel is a standard optimization routine that iteratively finds the best-fit sinusoid to match a suite of observed data. In this instance, "best-fit" was defined as finding the minimum root mean square error (RMSE). The Solver optimization routine was applied independently to both the clast inclination and clast ratio data. For the clast ratio data it was necessary to include an offset component to the optimization, since the clast ratio does not vary about zero. While the RMSE found the best-fit, one should also test for significance of the best-fit. To estimate significance we compared the standard deviation of the residuals with the amplitude of the best fit sinusoid found. In all cases the standard deviation of the residuals was greater than the amplitude of the best-fit sinusoid.

RESULTS

Clast Size

A plot of average clast size versus depth appears to suggest that a broad coarsening upward sequence (Fig. 3). There appears to be no definitive association between clast size and the lithological subdivisions summarized by Koeberl et al. (2007) for LB-07A. The variation of the standard deviation of clast size for each core segment shows a definite step near the top of the first suevite unit. Units below the first suevite have a lower value of standard deviation (Fig. 3). With two anomalous exceptions, units above the first suevite have a uniformly high standard deviation of clast size.

Plotting the grain-size data in terms of clast-size distribution provides a quite different impression (Fig. 4). The grain-size distribution appears to contain two zones: the deeper part of the core associated with the monomict lithic breccia, which is characterized by a narrow distribution of clast sizes; and the upper part, associated with the polymict lithic breccia and suevite units, generally characterized by a coarser clast size. Broader, more positively skewed grain-size populations (quite possibly reflecting the effect of multiple clast lithologies) also typify the upper zone. The grain size of the most frequent clast exhibits a systematic reduction in size with decreasing depth in the ejecta blanket (Fig. 4). The lower monomict lithic breccia is typified by a uniform clast size of around 10 mm. The contact between the monomict lithic breccia and the lowermost unit of suevite is marked by a sharp increase in clast size. The lowermost polymict lithic breccia horizon is also associated with a noticeable bimodal grain-size distribution. As noted above, the data was calculated on sample means irrespective of lithologic boundaries, yet the grain-size distribution data suggest that suevite and polymict lithic breccia units differ in terms of their grain-size distribution. The suevite units ppear to be associated with broader clast size distributions, whereas the polymict lithic breccias have more bimodal distributions.

Clast Ellipticity and Inclination

There are no big changes in the average ellipticity of the clasts (Fig. 3). For the most part the core segment from the monomict lithic breccia has lower ellipticity than the

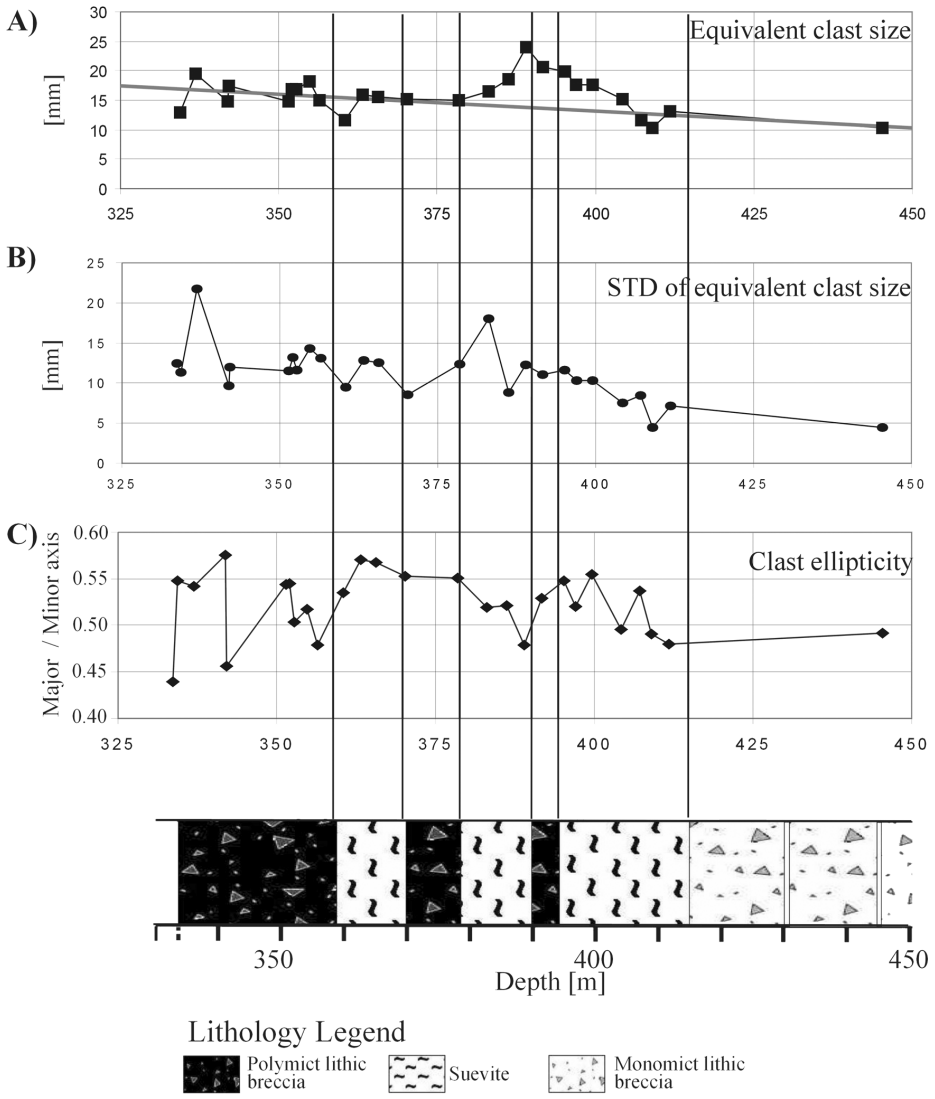

Fig. 3. A plot comparing core segment mean values for, respectively, (a) equivalent clast size (mm), (b) standard deviation of mean equivalent clast size (mm), and (c) mean clast ellipticity (dimensionless), computed as the ratio of major over minor axis. The dark gray line on the clast-size plot describes a simple linear increase in grain size with decreasing depth in the core. Lithological log from Koeberl et al. (2007).

segments taken from the overlying units of the polymict lithic breccia and suevite. The exception is the uppermost unit of polymict lithic breccia, which appears to have a systematically lower degree of ellipticity.

The plot of clast inclination suggests that there are identifiable systematic differences between the various lithological units (Fig. 5). The pattern of clast inclination changes at lithological boundaries. For the inclination convention we have adopted in this study a dipping fabric would be defined by two concentrations with equal and opposite inclination. Flat-lying fabrics would be defined by a single central concentration of inclination values. The lowermost monomict lithic breccia and the overlying suevite unit have a well-defined single population with a mean of around 0° indicative of a group of flat-lying clasts. (Note that there is a significant gap between the deepest core segment and the next one; see Table 1). There is a sharp boundary at the top of the first layer of polymict lithic breccia, which is associated with a mean inclination centered on zero but with a reduced concentration. The suevite unit from approximately 380 m to 390 m shows two strong groupings at approximately –30° and +30°. There are only a limited number of clasts having near zero inclination. Overlying this unit the polymict lithic breccia from 365 m to approximately 380 m shows a return to the strongly defined central grouping on near zero inclination. Finally, the uppermost unit of polymict lithic breccia again shows a return to a bimodal distribution of inclination values again at approximately 30° relative to the horizontal. This unit, however, contains a minor peak centered around an inclination of zero degrees.

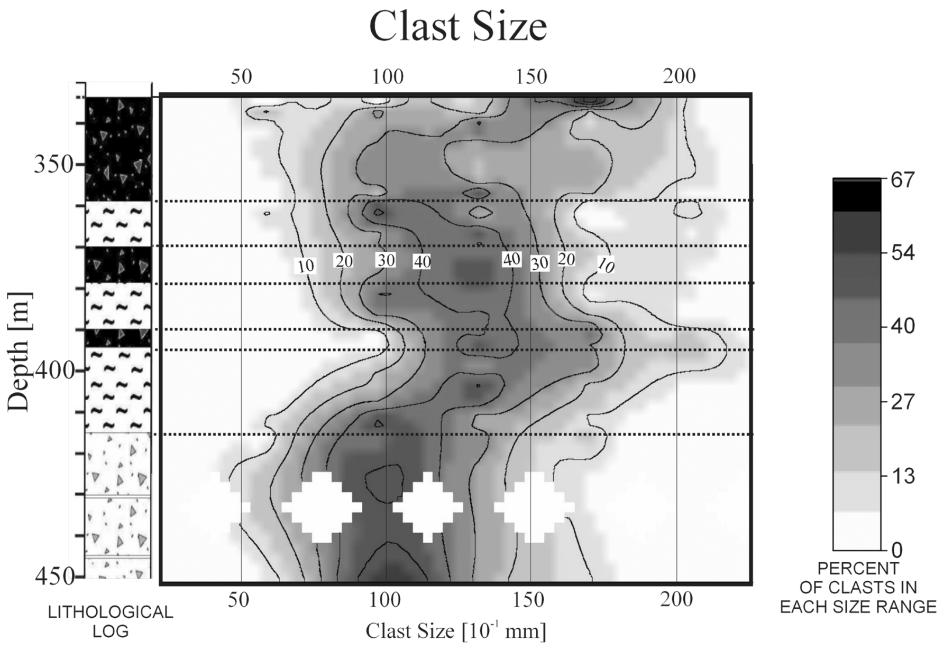

Fig. 4. A contour plot of variation of grain-size distribution with depth. Clast size distribution was grouped into a series of increasing groups. Actual clast sizes are in 10^{-4} m (10^{-1} mm). To eliminate the effect of varying number of clasts between core segments, the percentage of observations in each class is used. The contour plot was generated by gridding the grain-size distribution data for the 27 core segments examined using a minimum curvature gridding algorithm. The gaps in the data are produced because of lack of data in those intervals. Contour interval is 10%. The legend of the lithological log is the same as in Fig. 3. Lithological log from Koeberl et al. (2007).

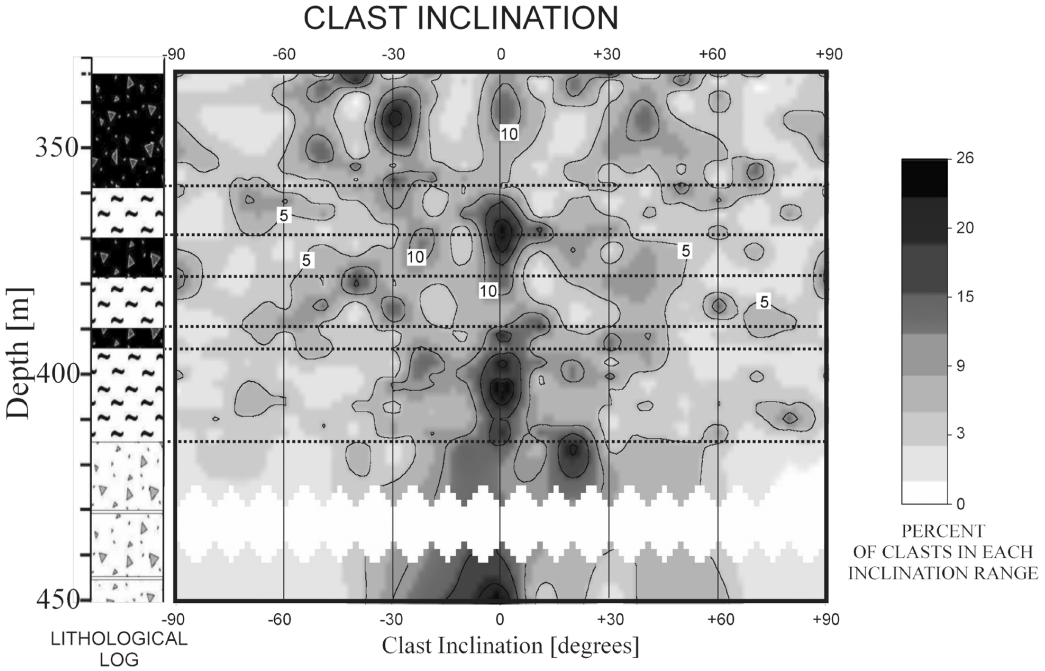

Fig. 5. A contour plot of variation of clast inclination distribution versus depth. Inclination is defined relative to the perpendicular to the long axis of the core. Therefore, an inclination of zero degrees represents a horizontal clast. Positive or negative values reflect orientation of dip relative to reference line on core. The clast inclination data was grouped into 10° increments relative to the long axis of the core segment. To eliminate the effect of the varying number of clasts between core segments, the percentage of observations in each class is used. The contour plot was generated by gridding the grain-size distribution data for the 27 core segments examined using a minimum curvature gridding algorithm. The gaps in the data are produced because of lack of data in those intervals. Contour interval is 5%. The legend of the lithological log is the same as on Fig. 3. Lithological log from Koeberl et al. (2007).

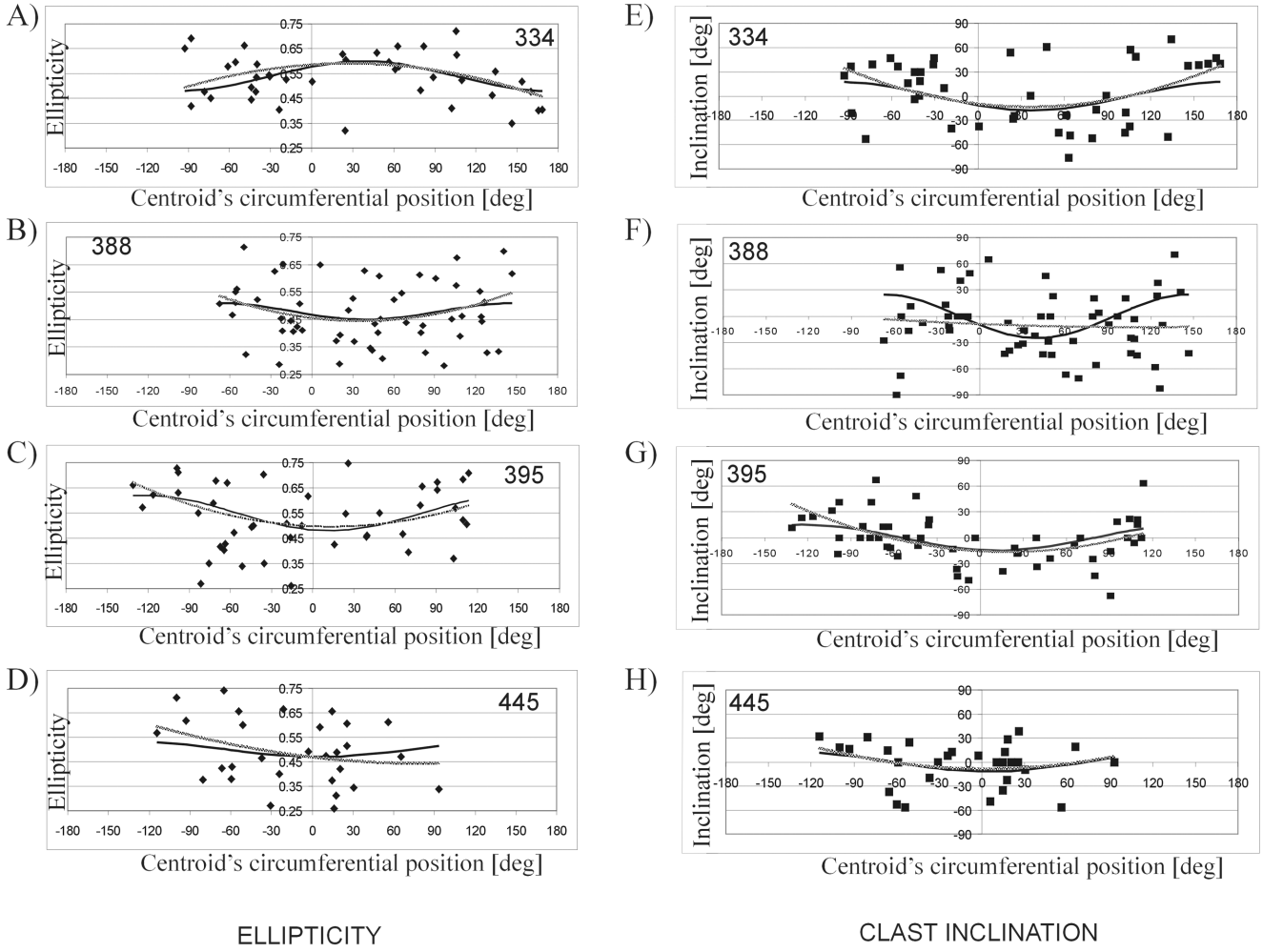

Fig. 6. Plots of variation of clast ellipticity (a–d) and clast inclination (e–h) versus circumferential position of class centroid for four core segments: i) depth 334 m, polymict lithic breccia (Figs. 6a and 6e); ii) depth 388 m, suevite (Figs. 6b and 6f); iii) depth 395 m, suevite/polymict lithic breccia (Figs. 6d and 6g); and iv) depth 445 m, monomict lithic breccia (Figs. 6d and 6h). Best-fit sinusoids calculated using an optimization routine embedded in Microsoft Excel are shown by a solid black line. Second-order polynomial line fit data is shown by a dotted line. All plots show large variation of observation about best-fit line. None of the calculated fits are statistically significant. See text for details.

Clast Fabric

If a strong single clast orientation is present, it should be apparent in both the clast inclination and clast ellipticity information. Figure 6 shows examples of data from three core segments investigated in this study. The three core segments represent four different lithologies from borehole LB-07A. Respectively, the four core segments represent: i) depth 445 m, monomict lithic breccia; ii) depth 395 m, suevite/polymict lithic breccia; iii) depth 388 m, suevite; and iv) depth 334 m, polymict lithic breccia. For the clast inclination data, in three of the four core segments the sinusoidal optimization routine shows a close similarity to the second order polynomial line fit, suggesting a well-defined fabric. The exception is core segment 388. As is visually apparent, this core segment exhibits a much broader distribution of observation points than any of the other core segments presented. As noted above, both of these parameters should show a sinusoidal variation with circumferential position. We outlined two tests to determine if a strong fabric is present, one based on a second order polynomial line fit, and a second based on an optimized least squares sinusoidal fitting routine. None of the polynomial line fits produced r^2 variations that were statistically significant. In all cases, the standard deviation of the residuals was greater than the amplitude of the best-fit sinusoid. The clast fabric data do not provide any definitive evidence for the clasts having a preferred orientation. The high degree of variation in clast inclination with circumferential position is more representative of a mixture of multiple clast directions. Core segment 334 provides the best example of a possible clast layering and is suggestive of a clast imbrication of around 20°.

CONCLUSIONS

In this study we examined the orientation and grain size of clast fragments within the impactite units sampled in Bosumtwi core LB-07A. The clast fabric parameters were derived from the full-core digital scans acquired at the ICDP facility in Potsdam, Germany, in 2004. Calculation of fabric parameters was derived from best-fit ellipsoid variations.

Masaitis (2005) has proposed that crater-fill deposits exhibit a broad three-fold subdivision. This study of core segments from borehole LB-07A suggests that the crater-fill material at the Bosumtwi impact site has a broad two-fold subdivision. The lower most segment comprising monomict lithic breccia and suevite is typified by the following characteristics: a) shallow and/or flat-lying clasts, b) lower clast ellipticity, c) lower and uniform clast size, and d) lower standard deviation in clast size. The uppermost segment comprising polymict lithic breccia and suevite is typified by the following characteristics: a) interbedding of layers having moderate clast fabric with layers having mixed, or no defined clast fabrics, b) increased and locally variable clast ellipticity, c) initially higher clast size which shows a complex variation with decreasing depth, and d) increased standard deviation of clast size.

Nowhere in this analysis have we differentiated clast fabrics on the basis of clast lithology. It is quite possible that much of the variation observed in the upper subdivision could be explained by the polymict nature of the lithic breccia. If examined in terms of a simple core segment average, the variation of clast size versus depth suggests a coarsening upward sequence. When plotted as clast size frequency distribution it becomes apparent that the highest concentration of clasts shows a decrease in size versus depth, that is, a fining upward sequence. This apparent discrepancy can be explained by the mixing of two sets of fragments having different grain size distributions. Theoretically, having sections through elliptical fragments should lead to a negatively skewed grain size distribution (Sahagian and Proussevitch 1998). Yet the upper section of this core shows a strongly positively skewed grain size distribution.

Contour plots of clast inclination data together with detailed analyses of data for individual core segments suggest that the deeper part of the impactite pile is characterized by flat-lying (horizontal) clasts having no obvious orientation. In the shallower section of the stratigraphic pile the clasts exhibit a poorly defined fabric, which has an inclination of around 20°. It was not possible to derive any directional estimate of the orientation of this weak fabric. With data from only one borehole it is not possible to establish the spatial variation of this fabric. Recognizing oriented fabrics in blocks from the Ries crater, Bringmeier (1994) has argued that these provide evidence for a period of "laminar flow" during deposition. The results we have obtained from the Bosumtwi samples, while indicating that planar fabrics can be detected, provide few constraints on the processes that may have lead to their genesis. Unfortunately, we are limited by having access to information from only one core. Ideally if it were possible to establish fabric patterns at a number of locations around the crater, then one might be able to obtain some discrimination of the relative importance of ballistic deposition versus ground surge, or the degree of post-impact adjustment of the breccia bodies (Deutsch, personal communication).

The clast orientation data is characterized by interbedding of zones with flat clast layering and zones having inclined clasts with no preferred orientation. The clast size distribution data suggests two distinct phases of clast deposition. While primarily evidenced by the change from monomict to polymict lithic breccia, this feature is also recorded by the morphology and orientation of the included clasts. There is nothing to indicate that any other process other than ballistic ejection and subsequent accumulation was involved in the formation of these crater-fill sediments.

Acknowledgments–Drilling at Lake Bosumtwi was supported by the International Continental Scientific Drilling Program (ICDP), the U.S. NSF-Earth System History Program under grant no. ATM-0402010, Austrian FWF (project P17194-N10), the Austrian Academy of Sciences, and by the Canadian Natural Sciences and Engineering Research Council (NSERC). Drilling operations were performed by DOSECC. Careful reviews of the original manuscript by Alex Deutsch and V. Masaitis have helped clarify some sections of the paper. Financial support for this project was provided by a SRO-NSERC research grant to W. A. Morris that was managed by Bernd Milkereit, University of Toronto. Bernd is also to be thanked for the substantive support he provided during the acquisition of this data.

Editorial Handling—Dr. Christian Koeberl

REFERENCES

Bringemeier D. 1994. Petrofabric examination of the main suevite of the Otting Quarry, Nördlinger Ries, Germany. *Meteoritics* 29: 417–422.

Coney L., Gibson R. L., Reimold W. U., and Koeberl C. 2007. Lithostratigraphic and petrographic analysis of ICDP drill core LB-07A from the Bosumtwi impact structure, Ghana. *Meteoritics & Planetary Science* 42. This issue.

Deutsch A., Luetke S., and Heinrich V. 2007. The ICDP Lake Bosumtwi impact crater scientific drilling (Ghana): Core LB-08A litho-log, related distal ejecta, and shock recovery experiments. *Meteoritics & Planetary Science* 42. This issue.

Ferrière L., Koeberl C., and Reimold W. U. 2007. Drillcore LB-08A, Bosumtwi impact structure, Ghana: Petrographic and shock metamorphic studies of rocks from the central uplift. *Meteoritics & Planetary Science* 42. This issue.

Hunze S. and Wonik T. 2007. Lithological and structural characteristics of the Lake Bosumtwi impact crater, Ghana: Interpretation of acoustic televiewer images. *Meteoritics & Planetary Science* 42. This issue.

Karatson D., Sztano O., and Telbisz T. 2002. Preferred clast

orientation in volcaniclastic mass-flow deposits: Application of a new photo-statistical method. *Journal of Sedimentary Research* 72:823–835.

Knauth L. P., Burt D. M., and Wohletz K. H. 2005. Impact origin of sediments at the Opportunity landing site on Mars. *Nature* 438: 1123–1128.

Koeberl C., Denison C., Ketcham R. A., and Reimold W. U. 2002. High-resolution X-ray computed tomography of impactites. *Journal of Geophysical Research* 107:1–9.

Koeberl C., Milkereit B., Overpeck J. T., Scholz C. A., Amoako P. Y. O., Boamah D., Danuor S. K., Karp T., Kueck J., Hecky R. E., King J., and Peck J. A. 2007. An international and multidisciplinary drilling project into a young complex impact structure: The 2004 ICDP Bosumtwi impact crater, Ghana, drilling project—An overview. *Meteoritics & Planetary Science* 42. This issue.

Krumbein W. C. 1939. Preferred orientation of pebbles in sedimentary deposits. *Journal of Geology* 47:673–706.

MacDonald W. D. and Palmer H. C. 1990. Flow directions in ash-flow tuffs: A comparison of geological and magnetic susceptibility measurements, Tshirege Member (upper Bandelier Tuff), Valles Caldera, New Mexico, USA. *Bulletin of Volcanology* 53:45–59.

Masaitis V. L. 2005. Morphological, structural, and lithological records of terrestrial impacts: An overview. *Australian Journal of Earth Sciences* 52:509–528.

Morris W. A., Ugalde H., and Clark C. 2007. Physical property measurements: Boreholes LB-07A, LB-08A, Lake Bosumtwi, Ghana. *Meteoritics & Planetary Science* 42. This issue.

Ort M. H., Rosi M., and Anderson C. E. 1999. Correlation of deposits and vent locations of the proximal Campanian ignimbrite deposits, Campi Flegrei, Italy, based on natural remanent magnetization and anisotropy of magnetic susceptibility characteristics. *Journal of Volcanology and Geothermal Research* 91:167–178.

Sahagian D. L. and Proussevitch A. A. 1998. 3-D particle size distributions from 2-D observations: Stereology for natural applications. *Journal of Volcanology and Geothermal Research* 84:173–196.